SELF-CONSISTENT ELECTRON CYCLOTRON RESONANCE ABSORPTION IN A PLASMA WITH VARYING PARAMETERS

by

M. C. Williamson, A. J. Lichtenberg, and M. A. Lieberman

Memorandum No. UCB/ERL M91/114

18 December 1991

SELF-CONSISTENT ELECTRON CYCLOTRON RESONANCE ABSORPTION IN A PLASMA WITH VARYING PARAMETERS

by

M. C. Williamson, A. J. Lichtenberg, and M. A. Lieberman

Memorandum No. UCB/ERL M91/114

18 December 1991

ELECTRONICS RESEARCH LABORATORY

College of Engineering
University of California, Berkeley
94720

SELF-CONSISTENT ELECTRON CYCLOTRON RESONANCE ABSORPTION IN A PLASMA WITH VARYING PARAMETERS

by

M. C. Williamson, A. J. Lichtenberg, and M. A. Lieberman

Memorandum No. UCB/ERL M91/114

18 December 1991

SELF-CONSISTENT ELECTRON CYCLOTRON RESONANCE ABSORPTION IN A PLASMA WITH VARYING PARAMETERS

by

M. C. Williamson, A. J. Lichtenberg, and M. A. Lieberman

Memorandum No. UCB/ERL M91/114

18 December 1991

ELECTRONICS RESEARCH LABORATORY

College of Engineering
University of California, Berkeley
94720

1 Introduction

Electron cyclotron resonance (ECR) sources have been applied to plasma etching and deposition of thin films in the past several years. As the use of ECR reactors has become more widespread, much research has focused on operating characteristics, which has revealed operating behavior not yet fully understood. One general configuration for plasma heating is to transmit the microwave power through a window into the microwave heating chamber, in which there is a decreasing magnetic field, with $\omega_{ce}(z) > \omega$ at the window, where ω_{ce} is the local cyclotron radian frequency and ω is the applied radian frequency. Within the plasma chamber, the fundamental components of the wave, for propagation parallel to the magnetic field B_0 and with a plasma present, are the right hand polarized (RHP) wave and left hand polarized (LHP) wave. For significant plasma density, the LHP wave is usually cutoff, while the RHP wave propagates and can be absorbed on a "magnetic beach" in the neighborhood of the cyclotron resonance $\omega_{ce}(z_{res}) = \omega$. The absorption of the RHP wave has application to many physical problems. It was studied by Budden [1] in connection with wave propagation and absorption in the ionosphere, and by Stix [3] in connection with the heating of fusion plasmas.

We briefly review the Budden theory of wave absorption. We begin with the wave equation for the electric field in one dimension for an RHP wave with collisional losses:

$$\frac{d^2}{dz^2}E + {k_0}^2\left[1 - \frac{\omega_p^2(z)}{\omega(\omega - \omega_{ce}(z) - j\nu(z))}\right]E = 0 \tag{1}$$

where $\omega_{ce}(z) \equiv eB(z)/m$, $\omega_p^2(z) = e^2 n_p(z)/m\epsilon_0$ is the square of the plasma frequency, $\nu(z)$ is the collision frequency, and $k_0 = \omega/c$ is the free space wavenumber. If ω_p and ν are constants independent of z, then linearizing ω_{ce} about the resonance point we obtain

$$\frac{d^2}{ds^2}E + \left[\frac{\omega_p^2/\omega c\alpha}{s + j\nu/c\alpha} + 1\right]E = 0 \tag{2}$$

where we have normalized z by $s = k_0(z - z_{res})$ and $\alpha = {B_0}^{-1}(dB/dz)_{z_{res}}$, where B_0 is B at resonance. This corresponds to the form investigated by Budden

$$\frac{d^2}{ds^2}E + \left[\frac{\eta}{s + i\gamma} + 1\right]E = 0 \tag{3}$$

with $\eta = \omega_p^2/\omega c\alpha$ and $\gamma = \nu/c\alpha$. The dielectric function has a pole and a zero, with the pole, in the absence of collisions, occurring at $s = 0$ ($z = z_{res}$) and the zero at $s = -\eta$. In the approximation of (3) Budden obtained solutions for waves traveling in either direction. For a wave traveling into a decreasing magnetic field (the magnetic beach) he calculates the transmission (tunneling) and reflection factors

$$T = e^{-\frac{1}{2}\pi\eta} \tag{4}$$

$$R = 0 \tag{5}$$

where $T = \mid E_{trans}/E_{fwd} \mid$ and $R = \mid E_{refl}/E_{fwd} \mid$. Since there is no reflected wave, the ratio of absorbed to forward power is given by

$$P_{abs}/P_{fwd} = 1 - T^2 = 1 - e^{-\pi\eta}. \tag{6}$$

For a wave traveling into an increasing magnetic field the solution gives both transmission *and* reflection

$$T = e^{-\frac{1}{2}\pi\eta} \tag{7}$$

$$R = 1 - e^{-\pi\eta}. \tag{8}$$

Since $T^2 + R^2 < 1$ there is absorption in this case also. When the normalized distance η between the pole and the zero is large compared to a wavelength far from resonance, no tunneling occurs and the reflection or absorption of the wave is determined by whether it encounters the pole or the zero first. When the pole-zero separation is small compared to a free space wavelength, significant tunneling occurs.

Considering the wave incident on a magnetic beach, the Budden theory predicts that most of the power will be absorbed for $\eta > 1$. Using the definition of η in (3) and taking a

typical case for which $\lambda_0 = 2\pi/k_0 \approx \alpha^{-1}$, we find that $\eta = 1$ corresponds to $\omega_p^2/\omega^2 \approx 1/2\pi$. Thus we expect the power to be absorbed at a density significantly below the critical density $\omega_p = \omega$.

Clearly, the Budden theory is too idealized for application to a physical system in a number of respects. The reflections in a plasma chamber generate interference of waves that can significantly affect the absorption. The variation of axial plasma density causes initial upstream power reflection not included in the Budden theory. The collisionality is strongly locally enhanced by nonlinear absorption of power in the resonance zone. These effects can be taken into account in a one-dimensional model by numerical integration of the fundamental equation (1). Boundary conditions may be imposed at each end of the chamber, with reflections modeled by a movable short at the chamber end (E-field null) and linearly polarized waves injected at the microwave source end (left-and right-hand polarized waves of equal magnitude and phase at the entrance window).

In addition, the waves are not propagating parallel to the magnetic field due to a nonzero transverse separation constant in a finite diameter cylindrical ECR chamber. This couples the fundamental RHP and LHP waves together, as well as with their extraordinary and ordinary wave counterparts for propagation perpendicular to B. Once the RHP wave is significantly absorbed, the density rises such that for the usual power inputs $\omega_p > \omega$. For this condition it has been shown [2, 4] that mode conversion at $\omega_p = \omega$ for a small but finite

transverse separation constant can give significant absorption of the LHP wave, which can lead to an additional increase in density by up to a factor of two for an incident linearly polarized wave, with a relatively small fraction of incident power being reflected. In this work we concentrate on the effects of an incident RHP wave alone, by considering only propagation parallel to B.

In Section 2 we present the numerical solution of a propagating wave of more general axial variation which can be compared with the analytic results. More realistic situations are then treated, including the effects of downstream reflections. In Section 3 we investigate the relationship between linear and nonlinear absorption to construct an effective collision frequency $\nu_{eff}(z)$ localized in the nonlinear resonance zone. This is used, together with a model density distribution, to determine field patterns and absorption. In Section 4, we describe simple ECR equilibrium dynamics, self-consistently treating the system power balance including energy gain by electrons in the resonance zone and energy losses to the walls. In Section 5, we present our conclusions.

2 Spatially Varying Wave Equation

We use the basic wave equation for a RHP wave propagating in an unbounded plasma with axially varying magnetic field and plasma density to obtain the complete wave solution for the propagating wave. From the resulting field solution the power and power derivative (absorption) are also obtained. The basic wave equation (1) with spatially varying coefficients is solved numerically by separating into real and imaginary parts. Defining $G = dE/ds$ and taking $E = E_R + iE_I$ and $G = G_R + iG_I$, we obtain four first-order ordinary differential equations:

$$dE_R/ds = G_R \tag{9}$$

$$dE_I/ds = G_I \tag{10}$$

$$dG_R/ds = (n^2)_I E_I - (n^2)_R E_R \tag{11}$$

$$dG_I/ds = -(n^2)_R E_I - (n^2)_I E_R \tag{12}$$

First we consider the normalized propagation constant $n = k/k_0$ obtained by linearization of B about resonance at constant density, as given in (3), to obtain

$$(n^2)_R = 1 + \frac{\beta s}{s^2 + \gamma^2} \tag{13}$$

$$(n^2)_I = -\frac{\beta\gamma}{s^2+\gamma^2} \tag{14}$$

Far from the resonance zone we can use the analytic solution, obtained by Budden [1], for the field, after propagation through resonance from the high magnetic field side:

$$E = \exp\{is + i\frac{\beta}{2}\log \mid s \mid + i\frac{\beta}{2}\log 2 - \frac{\pi\beta}{4}\}. \tag{15}$$

Equation (15) can be expanded in terms of real and imaginary parts of E and its derivative G to obtain

$$E_R = \exp\{-\frac{\pi\beta}{4}\}\cos\{s + \frac{\beta}{2}\log \mid 2s \mid\} \tag{16}$$

$$E_I = \exp\{-\frac{\pi\beta}{4}\}\sin\{s + \frac{\beta}{2}\log \mid 2s \mid\} \tag{17}$$

$$G_R = -\{1 + \frac{\beta}{\mid 2s \mid}\}E_I \tag{18}$$

$$G_I = \{1 + \frac{\beta}{\mid 2s \mid}\}E_R \tag{19}$$

Equations (9)–(14) can be solved numerically, together with (16)–(19). The numerical integration scheme is a standard fourth-order Runge-Kutta algorithm with an intelligently varying step size according to error tolerance requirements. The results for the transmission coefficient versus density are compared with the analytic result from (4) for $\nu \ll \omega$ where the analytic results are accurate, in Fig. 1, giving excellent agreement. We thus have confidence

to apply the numerical technique to obtain the variation of the field and transmitted power as a function of z, and to extend the method to general variations of $n_p(z)$, $B(z)$, and $\nu(z)$. Keeping in mind that $\omega_p = \omega$ for $n_p = 7.4 \times 10^{10}\,\mathrm{cm}^{-3}$ at a typical microwave frequency of $f = \omega/2\pi = 2.45\,\mathrm{GHz}$ and that $\nu = 10^9 \mathrm{s}^{-1}$ is quite large compared to the typical background collisionality in a normal ECR processing discharge ($\nu \cong 5.3 \times 10^7\,\mathrm{s}^{-1}$ at $p = 10\,\mathrm{mTorr}$), we plot the magnitude of the power as a function of normalized z with n_p as a parameter at $\nu = 10^9\,\mathrm{s}^{-1}$, and with ν as a parameter at $n_p = 10^{10}\,\mathrm{cm}^{-3}$ in Fig. 2a and b, respectively. The results clearly show that at high density or high collisionality, the transmitted power falls well before reaching the resonance position. As we shall see in Section 3, this result is consistent with a nonlinear calculation of power absorption at ECR resonance.

The field variation through the resonance region depends not only on the power absorption but also on the variation of the local wave impedance. This field has been calculated analytically by Stix [3] for the simplified case of a single pole (no zero) for vanishingly small collisionality. In Fig. 3 we compare the numerical results with the analytic calculation, in the neighborhood of the resonance, with collisionality as a parameter. As expected, we find excellent agreement for low collisionality but increasing deviation as the collisionality is increased.

We now consider a more realistic magnetic field and plasma profile, and the effect of wave solutions in which there are reflections and therefore RHP waves traveling in both directions

are present. Starting again with the wave equation (1) we choose a model in which

$$\omega_{ce}(z) = \omega(1 + \tanh(\alpha z)) \tag{20}$$

$$\omega_p^2(z) = \omega_{p0}^2(1 + \tanh(\alpha z)) \tag{21}$$

$$\nu(z) = \frac{\nu_m}{1 + 4z^2/\langle \Delta z \rangle^2} \tag{22}$$

where as before, $\alpha = B_0^{-1}(dB/dz)_{z_{res}}$. The density variation through the resonance zone follows the magnetic field strength variation, consistent with particles streaming along field lines. The axial profile of the collisionality parameter has been chosen to be a Lorentzian, which is large near the resonance zone, to correspond to the nonlinear absorption, with ν_m and the scale length $\langle \Delta z \rangle$ obtained from the nonlinear absorption calculation in Section 3. The new values of $(n^2)_R$ and $(n^2)_I$ in (9)–(12) are

$$(n^2)_R = 1 + \frac{\rho \tanh(\chi s)(1 + \tanh(\chi s))}{\tanh^2(\chi s) + \sigma^2(s)} \tag{23}$$

$$(n^2)_I = -\frac{\sigma(s)\rho(1 + \tanh(\chi s))}{\tanh^2(\chi s) + \sigma^2(s)} \tag{24}$$

where $\rho = \omega_{p0}^2/\omega^2$, $\chi = \alpha c/\omega$, and $\sigma(s) = \nu(s)/\omega$.

Initial conditions are found by taking $\tanh(\chi s)$ to its limit, either -1 for negative s or +1 for positive s, and then finding the real and imaginary parts of the dielectric constant.

For large negative s the factor $1 + \tanh(\chi s)$ goes to zero, and the solution is a simple uniform plane wave propagating in the vacuum ($\omega_p = 0$). For large positive s, ($\omega_p^2 = 2\omega_{p0}^2$), the dielectric function has both real and imaginary parts, and the solution is a uniform plane wave with a spatially decaying exponential factor. The initial conditions for integrating from negative s to positive s are therefore

$$E_R = \cos s \tag{25}$$

$$E_I = \sin s \tag{26}$$

$$G_R = -\sin s = -E_I \tag{27}$$

$$G_I = \cos s = E_R, \tag{28}$$

and the initial conditions for integrating from positive s to negative s are

$$E_R = \exp\{n_I s\} \cos\{n_R s\} \tag{29}$$

$$E_I = -\exp\{n_I s\} \sin\{n_R s\} \tag{30}$$

$$G_R = n_I E_R + n_R E_I \tag{31}$$

$$G_I = n_I E_I - n_R E_R \tag{32}$$

where

$$n_R = n_0 \cos\phi \tag{33}$$

$$n_I = n_0 \sin\phi \tag{34}$$

and

$$n_0 = \left(1 + \frac{4\omega_p^2(\omega_p^2 - 3\omega^2)}{\omega^2(9\omega^2 + \nu^2)}\right)^{\frac{1}{4}} \tag{35}$$

$$\phi = \frac{1}{2}\tan^{-1}\left(\frac{-2\omega_p^2\nu}{9\omega^3 + \omega\nu^2 - 6\omega_p^2\omega}\right). \tag{36}$$

This second set of initial conditions is complicated by the non-zero plasma frequency ω_p. If ω_p is set to zero in the above expressions for n and ϕ, the second set of initial conditions reduces to a simple form comparable to the first set.

Because of the interest in effects caused by various reflections in an ECR system, the calculation was performed with a short at a variable position beyond the resonance zone (past the zero). First, the usual calculation was made for RHP waves traveling in the left and right directions under the same conditions. Then the two solutions were matched at the short position by requiring that the transverse electric field go to zero at that point. To accomplish this, one of the solutions was scaled by a complex constant factor (magnitude and phase shift) so that the two solutions would add to zero at the short position. The sum

of the two solutions then yields a single profile for a wave entering the system, passing the pole and then the zero, reflecting from the short, and then returning through the resonance zone. This was done over a half-wavelength range of short positions to see the effects of moving the short position on absorption. If such a short is placed in a position which results in a field null at the resonance zone, the reduced field strength at the resonance results in lower absorption.

The magnitude of the electric field is plotted versus $s = k_0 z$, for three different short positions, in Figs. 4a-c. The calculations in these figures use values of $\alpha = 10.8\ \mathrm{m}^{-1}$, $\omega_{p0} = 1.5 \times 10^{10}$ rad/sec, $\nu_m = 4.01 \times 10^8\ \mathrm{sec}^{-1}$, and $\Delta z = 0.495$ cm. In each of these three figures, waves enter from the right, pass through the resonance zone at $s = 0$, continue to the left where they reflect off the short, and return through the resonance zone moving back to the right. The short position is past the left edge of the scale in each of the three figures, but the sharp field nulls which result from it are visible in the left half of each figure. The density and axial magnetic field strength follow a hyperbolic tangent shape [see Eqs. (20) and (21)], starting at low values on the left side, increasing through the resonance zone, and leveling off at high values on the right side of the figures. It is important to note that due to the change in density from low to high in going from the left side to the right side, waves of equal power will have a larger electric field magnitude on the left, where the density is low, than on the right, where the density is much higher. Since

$$P \propto E^2/Z_p \; ; \; Z_p = \sqrt{\mu_0/\epsilon_p}, \tag{37}$$

and

$$\epsilon_p = \epsilon_0 \left(1 + \frac{\omega_p^2}{\omega(\omega_{ce} - \omega)}\right), \tag{38}$$

for fixed power P we find $E \propto \epsilon_p^{-1/4}$. The dielectric function is larger where the density is higher, so the electric field strength is smaller by the above relation.

In the progression from Fig. 4a to Fig. 4c, the short position moves toward the left in small steps, $s_0 = -15.3$, -15.8, and -16.1, respectively. The positions of the field nulls, where the left-traveling and right-traveling waves most strongly cancel each other, are determined by the position of the reflecting short, where the field is zero. The field nulls occur at half-wavelength steps away from the short, and as the short position moves, the field nulls move with it. Hence the electric field minimum near the resonance zone moves toward the left from Fig. 4a to Fig. 4c. In Fig. 4a the electric field strength is larger on the right side, indicating that absorption is taking place in the resonance zone. In Fig. 4b, the short has moved to the left, in turn moving the electric field minimum closer to the resonance zone. Absorption still takes place, but the electric field strength is larger on the left than on the right, due to the dielectric effect discussed above. This progression continues into Fig.

4c, where the field null is very close to exact resonance, and the electric field strength on the left is even larger.

The field pattern on the right in each figure can be understood as a wave moving to the left which has the same strength in each of the three figures, and a weaker wave moving to the right. The strength of this right-traveling wave increases from Fig. 4a to Fig. 4c as less power is absorbed, resulting in more power being reflected back toward the source on the right. It can be seen that the average value of the field strength on the right is constant through the three figures, but that the voltage standing wave ratio (VSWR) is increasing from Fig. 4a to Fig. 4c, indicating that a higher percentage of power is being reflected as the field null moves closer to resonance. Thus, with a field null near the resonance, the absorption decreases significantly.

To see this effect more clearly, the corresponding percent power absorbed is plotted versus short position in Fig. 5. It is seen that the absorption is strong over most short positions, but that it dips sharply over narrow, spatially periodic ranges of short positions. This behavior is explained by the occurrence of field nulls at half-wavelength intervals from the short position, as was seen in Figs. 4a-c. The corresponding points for each of Figs. 4a-c are noted in Fig. 5, showing that the percent power absorbed in Fig. 4c is half of that in Fig. 4a, a large change in absorption over a small change in short position. It should also be noted that if the short position is held fixed but the density is varied, field nulls will change position. This

is due to the variation of the wavelength with density.

A second type of reflection in an ECR system arises from the transition from the microwave window into the plasma. A relatively sharp rise in plasma density near the window can cause a significant fraction of the incoming power to be reflected before it enters the plasma. At low pressures this effect can be modeled as a plane wave reflection at a planar boundary between two regions of differing dielectric constants. To see the general effect we consider a plane wave in a vacuum region (dielectric constant $\epsilon = \epsilon_0$) normally incident on a region of finite density and corresponding dielectric constant. The resulting transmission coefficient at the window is

$$T_w = P_{trans}/P_{inc} = \frac{4\sqrt{\epsilon_r}}{(\sqrt{\epsilon_r}+1)^2} \tag{39}$$

where

$$\epsilon_r = \epsilon/\epsilon_0 = 1 + \frac{\omega_{pw}^2}{\omega(\omega_{ce}-\omega)} \tag{40}$$

is the relative dielectric constant for the RHP wave and $\omega_{pw}^2 = e^2 n_w/\epsilon_0 m$ is the square of the plasma frequency just beyond the window. Multiplying the transmission coefficient by the Budden power absorption factor (6), we obtain a composite ratio P_{abs}/P_{inc} of absorbed power to incident power. Defining a parameter K that is independent of the absolute density,

$$K = \frac{c\alpha}{(\omega_{cew} - \omega)} \frac{\omega_{pw}^2}{\omega_{pr}^2} \tag{41}$$

where ω_{pr} is the plasma frequency at the resonance, we obtain a family of curves P_{abs}/P_{inc} versus η for various values of K, which are plotted on a logarithmic scale in Fig. 6. The maximum of absorption is broad and lies near $\eta = 1$ for a practical range of values of the parameter K. From Fig. 6 it can be seen that the fractional power absorbed falls toward small densities due to the Budden factor. For a given K the fraction of power absorbed falls again toward higher densities as less power reaches the resonance zone due to the reflection at the window.

An alternative situation at higher pressures is a gradual rise in plasma density from the window to the central density. A density profile that can model this situation is

$$n(z) = \frac{n_0}{2}\left[1 + \tanh\left(\frac{z}{L}\right)\right], \tag{42}$$

where the parameter L is the scale length of the profile. Such a "transition layer" has been analyzed by Ginzburg [2], with the transmission coefficient given by

$$P_{trans}/P_{inc} = 1 - \frac{\sinh^2\left(S\left[\sqrt{1+\Gamma} - 1\right]\right)}{\sinh^2\left(S\left[\sqrt{1+\Gamma} + 1\right]\right)}, \tag{43}$$

where $S = \pi^2 L/\lambda$, λ is the free space wavelength and

$$\Gamma = \frac{\omega_{pw}^2}{\omega(\omega_{ce} - \omega)}. \tag{44}$$

where $\omega_{pw}^2 = e^2 n_w / \epsilon_0 m$, and n_w is the density just beyond the window. Equation (43) can be used along with (6) to determine the variation of P_{abs}/P_{inc} with density, for the gradual transition, with L/λ as a parameter, giving similar results to those shown in Fig. 6.

We emphasize that the preceding simple calculations are not meant to give absorptions for actual devices, but rather to highlight the interaction between the tendency toward increased ECR absorption at the higher densities and the counter-tendency of increased reflections at the vacuum-plasma interface. In an actual device the complete matching problem, including other discontinuities, must be considered.

3 Nonlinear Absorption and Effective Collisionality Near Resonance

Nonlinear Absorption. Electrons may enter the resonance zone from either the high field or low field side. The average energy gain of a single electron traversing the resonance zone is shown in Appendix A to be

$$\mathcal{E}_g = \frac{1}{2}m\left(\frac{e}{m}Et_e\right)^2 \tag{45}$$

where E is the RHP electric field amplitude in the resonance zone (assumed constant), t_e is the effective time spent in the resonance zone,

$$t_e = (2\pi/u_z\omega\alpha)^{\frac{1}{2}}\,, \tag{46}$$

and u_z is the parallel velocity at resonance, assumed constant over the resonance zone. An effective zone width can then be defined as

$$\Delta z = u_z t_e = (2\pi u_z/\omega\alpha)^{1/2}. \tag{47}$$

The power per unit area is found by integrating (45) over the flux of electrons incident on the zone:

$$P_{NL} = \int \mathcal{E}_g u_z f(u_z) du_z, \tag{48}$$

where f is the electron velocity distribution. Using (45) in (48) yields

$$P_{NL} = \frac{1}{2} \frac{E^2}{Z_0} \frac{2\pi\omega_p^2}{\omega c \alpha}, \tag{49}$$

where $Z_0 = (\mu_0/\epsilon_0)^{1/2}$ is the free space impedance. A similar result, for u_z turning in the resonance zone, has been obtained by Jaeger et al [7], giving slightly different scaling.

Collisional Absorption. We note that (49) is independent of u_z. This suggests that we can examine the $u_z \to 0$ limit in considering the effects of electron collisions. Adding a collisional (friction) term to the force equation, letting $\vec{E} = \Re\mathrm{e}\{(\hat{x} - j\hat{y})Ee^{j\omega t}\}$, and solving for the transverse velocity amplitudes, we obtain

$$u_{x0} + j u_{y0} = -\frac{2eE}{m} \frac{1}{\nu_m + j(\omega - \omega_{ce})}. \tag{50}$$

where ν_m is the electron momentum transfer frequency. The power absorbed per electron is

$$p_{ECR} = \frac{1}{2} \Re\mathrm{e}\left\{-eE_{x0}u_{x0}^* - eE_{y0}u_{y0}^*\right\}. \tag{51}$$

Substituting (50) in (51) with $E_{x0} = E, E_{y0} = -jE$, we find

$$p_{ECR} = m\left(\frac{eE}{m}\right)^2 \frac{\nu_m}{\nu_m^2 + (\omega - \omega_{ce})^2}. \tag{52}$$

To obtain the total heating power, we average (52) over the distribution of electrons near the resonance zone. Using the linear expansion near resonance

$$\omega_{ce}(z) = \omega(1 + \alpha z), \tag{53}$$

in (52), we obtain

$$p_{ECR} = \frac{e^2E^2}{m} \frac{\nu_m}{\nu_m^2 + \omega^2\alpha^2z^2} \tag{54}$$

Multiplying (54) by $n\,dz$ and integrating from $z = -z_0$ to $z = z_0$, we obtain

$$P_{ECR} = \frac{2e^2E^2n}{m\omega\alpha}\tan^{-1}(\omega\alpha z_0/\nu_m). \tag{55}$$

The total power absorbed is obtained by letting $z_0 \to \infty$ such that $\tan^{-1} \to \pi/2$ and (55) reduces to (49). We see that the power absorbed is independent of ν_m for constant electric field, and the nonlinear and collisional power absorption correspond. However, recognizing that most power is absorbed near the resonance zone, if we insert $z_0 \equiv \Delta z$, from (47), in (55) we find that for $\nu_m \ll \omega\alpha\Delta z$ almost all of the power is absorbed in the resonance zone.

Thus at low collisionality, the correspotween the collisional and the nonlinear power absorption remains.

Effective Collisionality. We wish tcollisional formalism when the collisionality is, in fact, described by an effective cequency from the nonlinear processes, rather than from real collisions. To do this the ansatz that half of the total power is absorbed in the resonant zone Δz, sthere is an effective ν_m in that region given, from (55), by

$$\langle\Delta z\rangle \tag{56}$$

where $\langle\Delta z\rangle$ is an effective zone width averaging (47) over a Maxwellian

$$\langle\Delta z\rangle = \langle 06\left(\frac{kT}{\omega^2\alpha^2 m}\right)^{\frac{1}{4}}. \tag{57}$$

Substituting (57) in (56) we obtaintive collisionality at exact resonance

$$\nu_m = \frac{^2\alpha^2 kT}{m}\Bigg)^{\frac{1}{4}} \tag{58}$$

Taking typical values of $\omega = 2\pi \times 2.45$ and $T = 5$ eV we find $\nu_m = 4.01 \times 10^8\ \mathrm{s}^{-1}$, and from (57), $\langle\Delta z\rangle = 0.495$ cm. We ahat (58) can be written as $\nu_m = 4.44\langle t_e\rangle^{-1}$, where $\langle t_e\rangle$ is the effective time spent ice, a physically appealing result.

In order to make the collision frequency local, we also add a shape factor such that the collisionality falls off to half of its peak value over the range $\pm\langle\Delta z\rangle/2$

$$\nu(z) = \frac{\nu_m}{1 + 4z^2/\langle\Delta z\rangle^2}. \tag{59}$$

We have used this form in (22) as the effective collision frequency for our numerical calculations presented in Figs. 4 and 5.

Comparison of Linear and Nonlinear Absorption. The nonlinear power absorption P_{NL} in (49) can be compared with the linear absorption P_L in the weak absorption limit by expanding (6) for small η to obtain

$$P_{abs} = \pi \frac{E_0^2}{Z_0} \frac{\omega_p^2}{\omega c \alpha} \tag{60}$$

where we have substituted E_0^2/Z_0 for P_{fwd}, where E_0 is the incident electric field. Comparing (49) and (60), we see that in the weak absorption limit the results agree if $E/E_0 = 1$, thus verifying the accuracy of the linear analysis.

For stronger absorption, the power absorbed saturates, as described by (6). For consistency in this case the resonant field must also decrease. For the high collisionality case $\nu = 10^9\ \mathrm{s}^{-1}$ plotted in Fig. 2a, we see that this is exactly what happens; the power flow at resonance for high absorption ($n_p = 10^{10}\ \mathrm{cm}^{-3}$) is $P_r \approx 0.3 P_{fwd}$. However, from Fig. 3 it is

seen that this decrease in P_r is a function of the collisionality, with the large decreases only occurring for large ν ($\nu \sim \omega$). This has led us to consider an effective high collisionality in the neighborhood of the resonance itself, given by (59).

For higher absorption, using the prescription for localized power absorption, we can also find the power flow and the electric field at resonance. Equating the nonlinear and linear power absorption from (49) and (6)

$$\frac{E^2}{Z_0}\pi\eta = \frac{E_0^2}{Z_0}\left(1 - e^{-\pi\eta}\right) \tag{61}$$

we can solve for the ratio of the effective electric field at resonance E_{eff} to the incident electric field E_0,

$$\frac{E_{eff}}{E_0} = \left(\frac{1 - e^{-\pi\eta}}{\pi\eta}\right)^{1/2}. \tag{62}$$

We can compare E_{eff} to the actual field at resonance, which might reasonably approximate the value of the effective constant field that would be used in a nonlinear calculation. This is done in Fig. 7 with the x's the values of E_{eff} calculated from (62) and the o's the values of the electric field at resonance. The correspondence is within a factor of two over much of the range, but fails at very high densities where the power is essentially all absorbed before resonance. In this region it would be necessary to redefine $\langle \Delta z \rangle$ and ν_m

self-consistently with the decay of the field. However the assumption that the electric field is a constant over the region of nonlinear absorption, which is used in the nonlinear calculation, is inappropriate in this high density regime, so the usefulness of such a calculation is not clear.

4 Equilibrium Power Balance

To obtain a fully self-consistent equilibrium, the density must be obtained from power balance in a particular physical system. A complete calculation would necessarily involve both the RHP and LHP waves, reflections at discontinuities, and effects of the transverse boundaries. Such a complete treatment is beyond the scope of our investigation of the RHP absorption. Nevertheless, it is instructive to make a power balance calculation to understand the qualitative features of the equilibrium.

Consider a given absorbed power P_{abs} per unit area. This power is lost through various channels, including electron and ion kinetic energy loss to the walls, excitation energy, elastic scattering collisional losses inside the plasma, and losses due to ionization, all of which balance the input power at the equilibrium ion density. The power balance equation is

$$P_{abs} = 2n_i u_i e\mathcal{E}_L \tag{63}$$

where $n_i u_i$ is the mean ion flux at the two end walls of the ECR discharge and $e\mathcal{E}_L$ is the effective energy lost per electron-ion pair created within the region. $\mathcal{E}_L$ (in volts) is the sum of the collisional electron energy lost through the channels listed above and the kinetic energy lost by electrons and ions at the end walls. $\mathcal{E}_L$ is generally a function of the electron temperature through the cross sections for collisional excitation and ionization processes and because the electron and ion kinetic energies are functions of T_e. For a typical processing discharge in argon with electron temperatures near 5 eV, the energy loss $\mathcal{E}_L$ is typically of order 70 eV [5]. The characteristic ion loss velocity can be estimated to be the Bohm velocity

$$u_i \approx u_B = \left(\frac{eT_e}{M}\right)^{1/2}. \tag{64}$$

Assuming all the power is in the RHP wave, we plot (6) and (63) to obtain a graph as shown in Fig. 8. Both functions are shown as normalized to P_{fwd}, which leaves (6) as a single exponential curve, and (63) as a straight line whose slope depends on P_{fwd}. Three such "load lines" are plotted, along with the corresponding values of the forward power. The equilibrium density and power are given by the intersection of the two curves. Similarly, equating (6) and (63) results in an expression for forward power as a function of the corresponding equilibrium density:

$$P_{fwd} = \frac{Cn_p}{1 - e^{-Bn_p}} \tag{65}$$

where $C = 2u_i e\mathcal{E}_L$ and $Bn_p = \pi\eta$. Equation (65) gives, for a given density, the forward power required to sustain that density in an equilibrium situation. Since (65) gives a finite $P_{fwd} = P^* = C/B$ at zero density, the implication is that this minimum input power is required for a steady-state plasma equilibrium to exist. This is plotted as the leftmost load line, which lies just tangent to the exponential curve at zero density.

From (65) and (39), for the reflection at the window, we can obtain a series of normalized plots of density versus incident power for various values of the parameter K in (41). This is equivalent to sweeping the forward power through a range of values, and so moving the load line in Fig. 8 across the exponential absorption curve, and plotting the series of intersecting points. When $K = 0$, there is no reflection at the window, and the forward power equals the incident power. This is the top curve in Fig. 9, which displays the normalized density parameter η versus the normalized incident power P_{inc}/P^* on logarithmic axes. The power P^* is the minimum power to sustain an equilibrium plasma:

$$P^* = 2u_i\mathcal{E}_L\omega c\alpha\epsilon_0 m/\pi e. \tag{66}$$

Fig. 9 shows that as incident power is increased, the density first rises exponentially, and

then rises nearly linearly, when the percent absorption is high. However, as the density at the window is increased (increasing K) the rate of increase in density with incident power is slowed due to reflection at the window.

5 Conclusions

ECR microwave power absorption depends not only on the local density within the chamber, but also on the field strength at the resonance position. We have shown that the placement of a field null near resonance can reduce absorption strongly. Such a field null could arise somewhat unpredictably due to various reflections inside the chamber. Since the wavelength is dependent on the local density of the plasma, interference nulls could also vary with the density, which is in turn dependent on the strength of absorption. These interdependencies make deterministic predictions difficult. This effect can be mitigated by designing an ECR system with a resonance zone which is larger than a typical field null or by designing the chamber to minimize reflections.

In general, absorption increases with increasing density, but if the density near the window where power enters the chamber is large and rises sharply, significant power can be reflected before entering the plasma. Because of these two competing effects, there is a broad maximum near the density parameter $\eta = 1$ at which power is optimally absorbed by the system. This is seen in the family of curves displayed in Fig. 6.

We have shown that the nonlinear power absorption by an electron in the resonance zone and the collisional heating power can be brought into correspondence with each other at low absorption. At higher absorption this correspondence can still be approximately achieved

by choosing an axial variation of the effective collisional momentum transfer frequency that has a pronounced maximum near resonance. The resulting decay of the electric field in the neighborhood of the resonance achieves this approximate correspondence.

We have introduced an equilibrium model in which the power loss is proportional to the density. Thus at low densities in which the ratio of absorbed to incident power is related linearly to the density there is a minimum power required for a steady-state plasma to exist, given in (66).

The theoretical results that we have obtained agree qualitatively with some heretofore puzzling experimental observations [8]. The downstream standing waves at low density (weak absorption), which disappear at higher density (strong absorption), correspond approximately to the experimental observations. The sharp drop in density (and therefore power absorption), at a particular value of input power, qualitatively agrees with the prediction embodied in Fig. 8. However, the value of density at which this occurs is not in quantitative agreement with the experimental observation [8]. Also, the residual persisting low density plasma at lower input power, observed experimentally, is not explained, although some hint of an explanation may be found in the complex interaction between density and internal reflections. The effect of transverse wave numbers and the consequent coupling of the RHP and LHP waves may also be important and indicates an area for further investigations.

A Nonlinear and Collisional Power Absorption

The transverse energy gained by an electron in one pass through a resonance zone can be calculated either for constant velocity in the zone [6] or for turning within the zone [7]. Although both types of trajectories occur for a collisional plasma with an isotropic velocity distribution, the results for the constant parallel velocity are characteristic and we will outline the derivation here. The complex force equation for the transverse velocity can be written in the form

$$\frac{du_r}{dt} - j\omega_{ce}(z)u_r = -\frac{e}{m}Ee^{j\omega t}, \tag{67}$$

where E is the amplitude of the RHP wave with $\vec{E} = \Re\mathrm{e}\{(\hat{x} - j\hat{y})Ee^{j\omega t}\}$. We expand the magnetic field near resonance as

$$\omega_{ce}(z) = \omega(1 + \alpha z) \tag{68}$$

where z is the distance from exact resonance. We approximate $z(t) \approx u_z t$, where u_z is the parallel velocity at resonance. Using (68) and substituting $u_r = u_{r0}\exp(j\omega t)$ into (67) we obtain

$$\frac{du_{r0}}{dt} - j\omega\alpha u_z t u_{r0} = -\frac{e}{m}E. \tag{69}$$

Integrating (69) from $t = -T$ to $t = T$, we obtain

$$u_{r0}(T)e^{-j\theta(T)} = u_{r0}(-T)e^{-j\theta(-T)} - (eE/m)\int_{-T}^{T} dt' e^{-j\theta(t')}, \tag{70}$$

where

$$\theta(t) = \omega\alpha u_t t^2/2. \tag{71}$$

In the limit $T \gg (2\pi/\omega\alpha u_z)^{1/2}$, the integral in (70) is

$$\int_{-T}^{T} dt' e^{-j\theta(t')} = (\pi/\omega\alpha u_z)^{1/2}(1-j). \tag{72}$$

Inserting (72) into (70), multiplying (70) by its complex conjugate, and averaging over the initial "random" phase $\theta(-T)$, we obtain

$$|u_{r0}(T)|^2 = |u_{r0}(-T)|^2 + (eE/m)^2(2\pi/\omega\alpha u_z). \tag{73}$$

The energy gain per pass is thus

$$\mathcal{E}_g = \frac{1}{2}m\left(\frac{eE}{m}\right)^2 t_e^2 \tag{74}$$

where t_e is the effective time in resonance

$$t_e = (2\pi/\omega\alpha u_z)^{1/2}. \tag{75}$$

The effective resonance width is

$$\Delta z = u_z t_e = (2\pi u_z/\omega\alpha)^{1/2}. \tag{76}$$

We can understand the form of t_e as follows: an electron passing through the zone coherently gains energy for a time t_e such that

$$[\omega - \omega_{ce}(u_z t_e)]\, t_e \approx 2\pi \tag{77}$$

Inserting (68) into the preceding equation and solving for t_e, we obtain (75).

Acknowledgements

The work was partially supported by DOE Grant No. DE-FG03-87ER1327 and NSF Grant No. ENG 87-10988.

References

[1] K.G. Budden, *Radio Waves in the Ionosphere*, pp 474-479 (Cambridge University Press, 1966).

[2] V.L. Ginzburg, *The Propagation of Electromagnetic Waves in Plasmas*, Ch. 3, Sec. 11, pp 94-118 (Addison-Wesley, 1964).

[3] T.H. Stix, *The Theory of Plasma Waves*, Secs. 10.1-10.7, pp 235-250 (McGraw-Hill, 1962).

[4] J. Musil and F. Zacek, Plasma Phys. **12**, 17 (1970); Plasma Phys. **13**, 471 (1971).

[5] G.R. Misium, A.J. Lichtenberg, and M.A. Lieberman, J. Vac. Sci. Technol. A **7**, 1011 (1989).

[6] A.F. Kuckes, Plasma Phys. **10**, 367 (1968).

[7] F. Jaeger, A.J. Lichtenberg, and M.A. Lieberman, Plasma Phys. **14**, 1073 (1972).

[8] D.A. Carl, M.C. Williamson, M.A. Lieberman, and A.J. Lichtenberg, J. Vac. Sci. Technol. B **9**, 339 (1991).

List of Figures

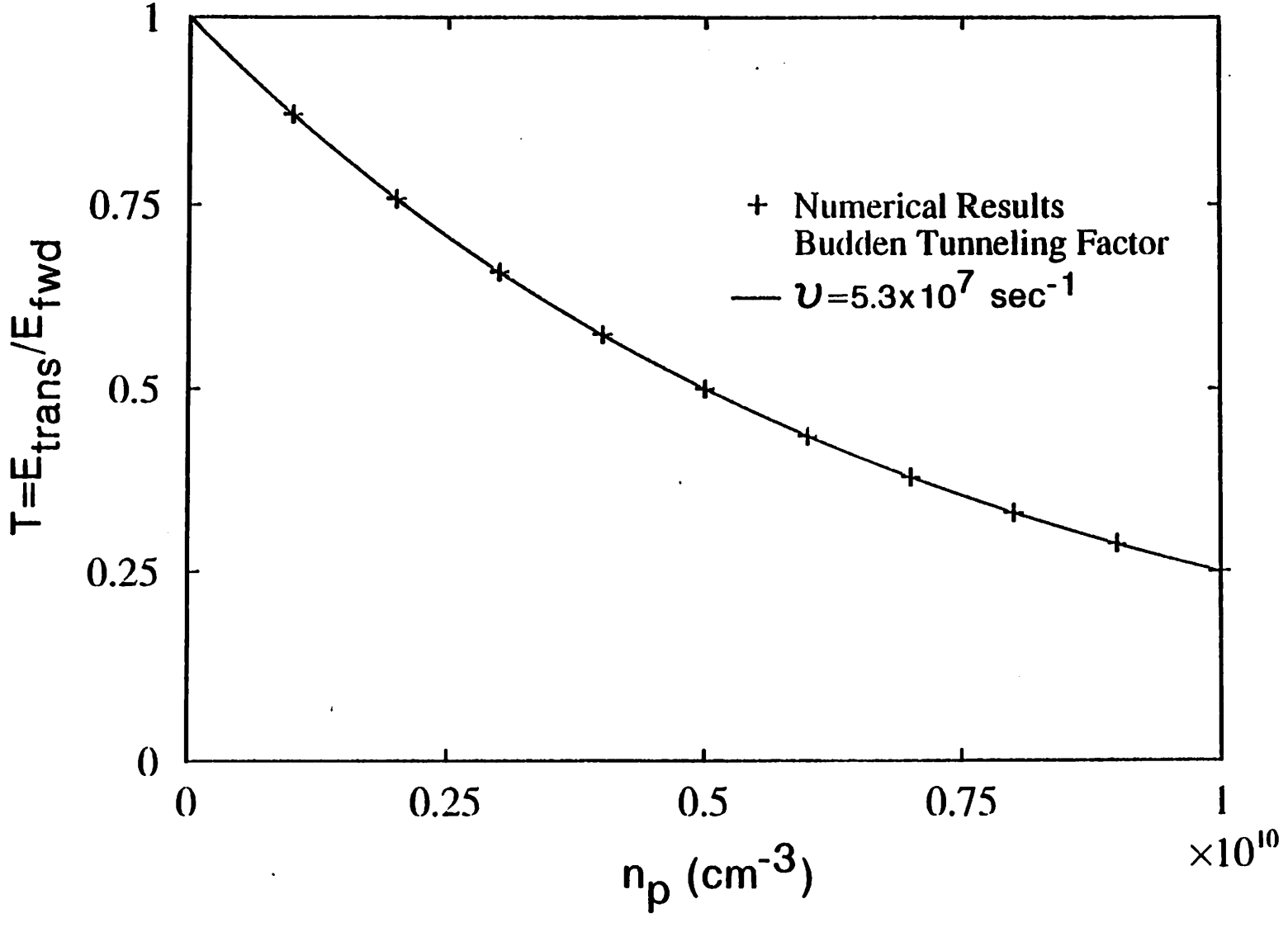
1
0.75
0.5
0.25
0
0
0.25
0.5
0.75
1
×10^10
T=E_trans/E_fwd
n_p (cm^-3)
+ Numerical Results
Budden Tunneling Factor
υ=5.3x10^7 sec^-1

Figure 1

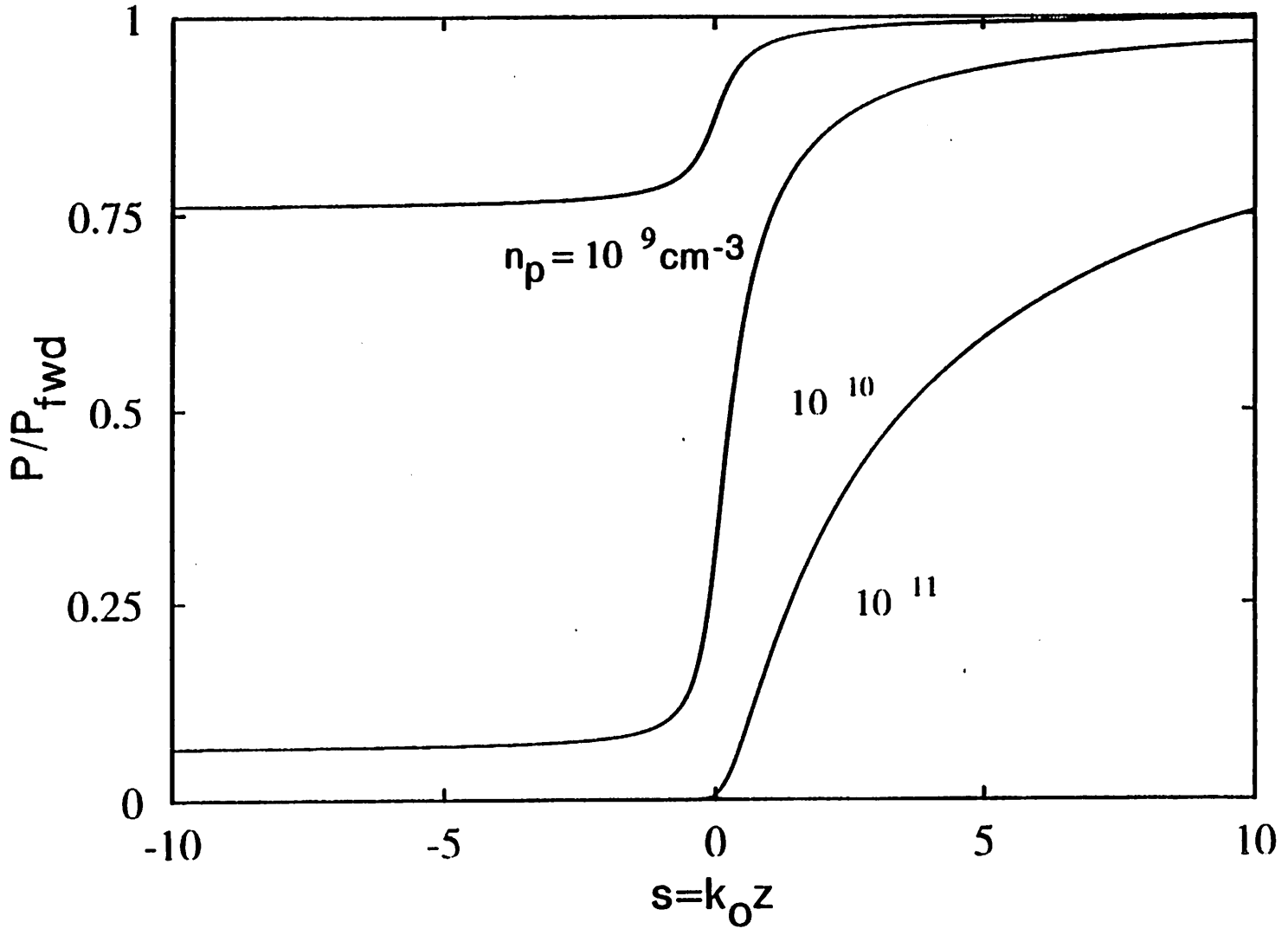

Figure 2a

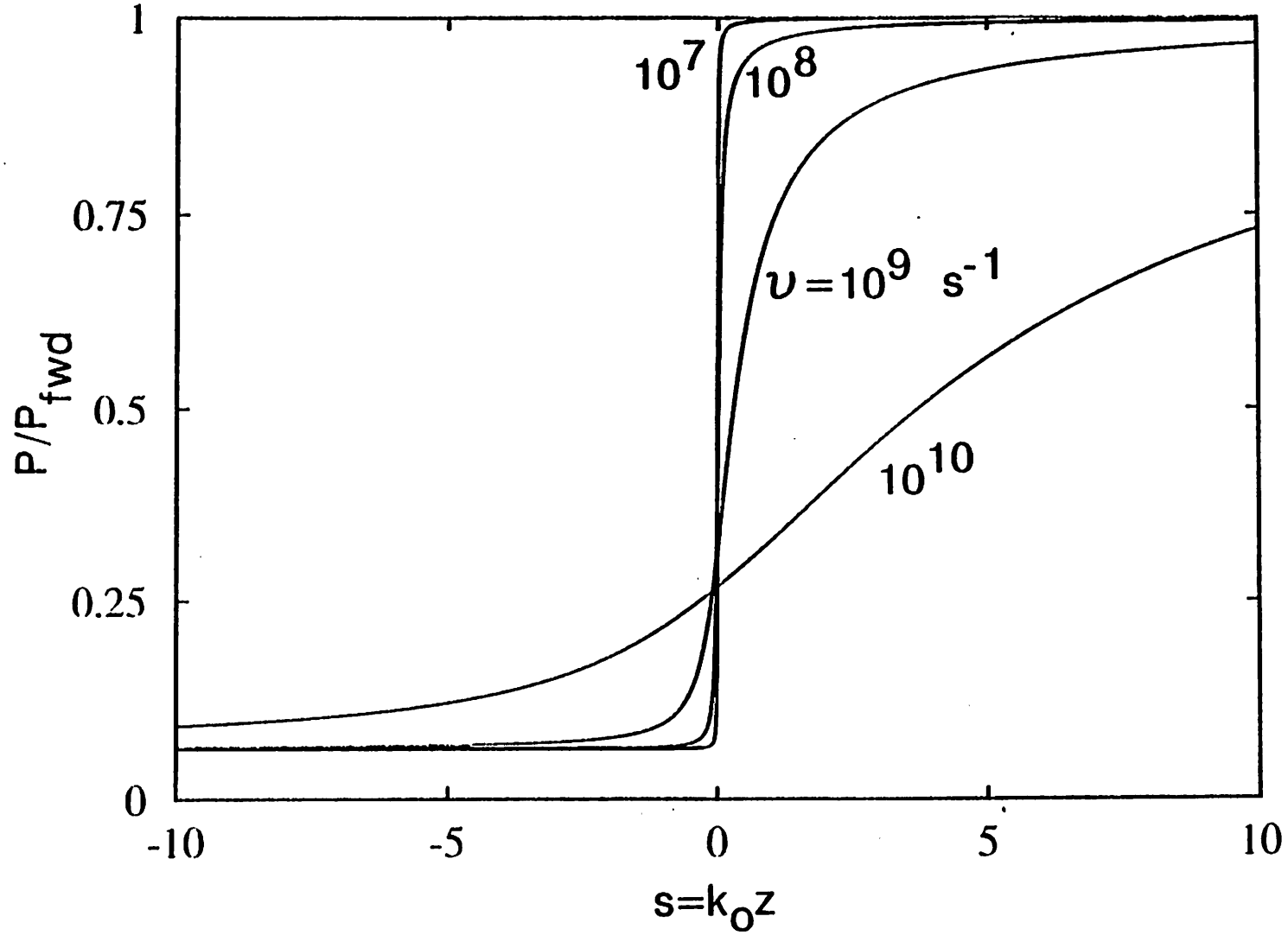

Figure 2b

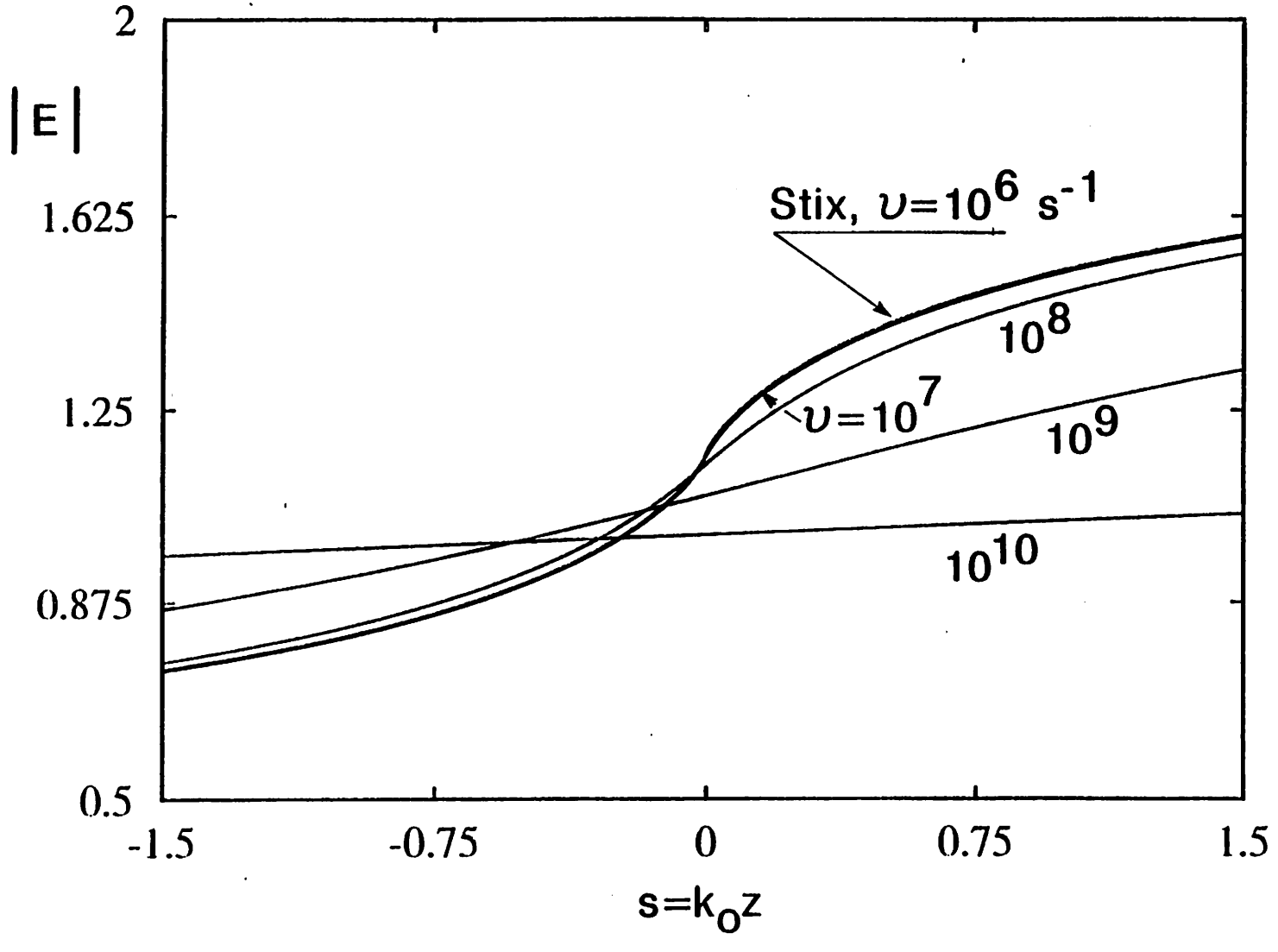
2
|E|
1.625
1.25
0.875
0.5
-1.5
-0.75
0
0.75
1.5
s=k0z
Stix, υ=10^6 s^-1
10^8
υ=10^7
10^9
10^10

Figure 3

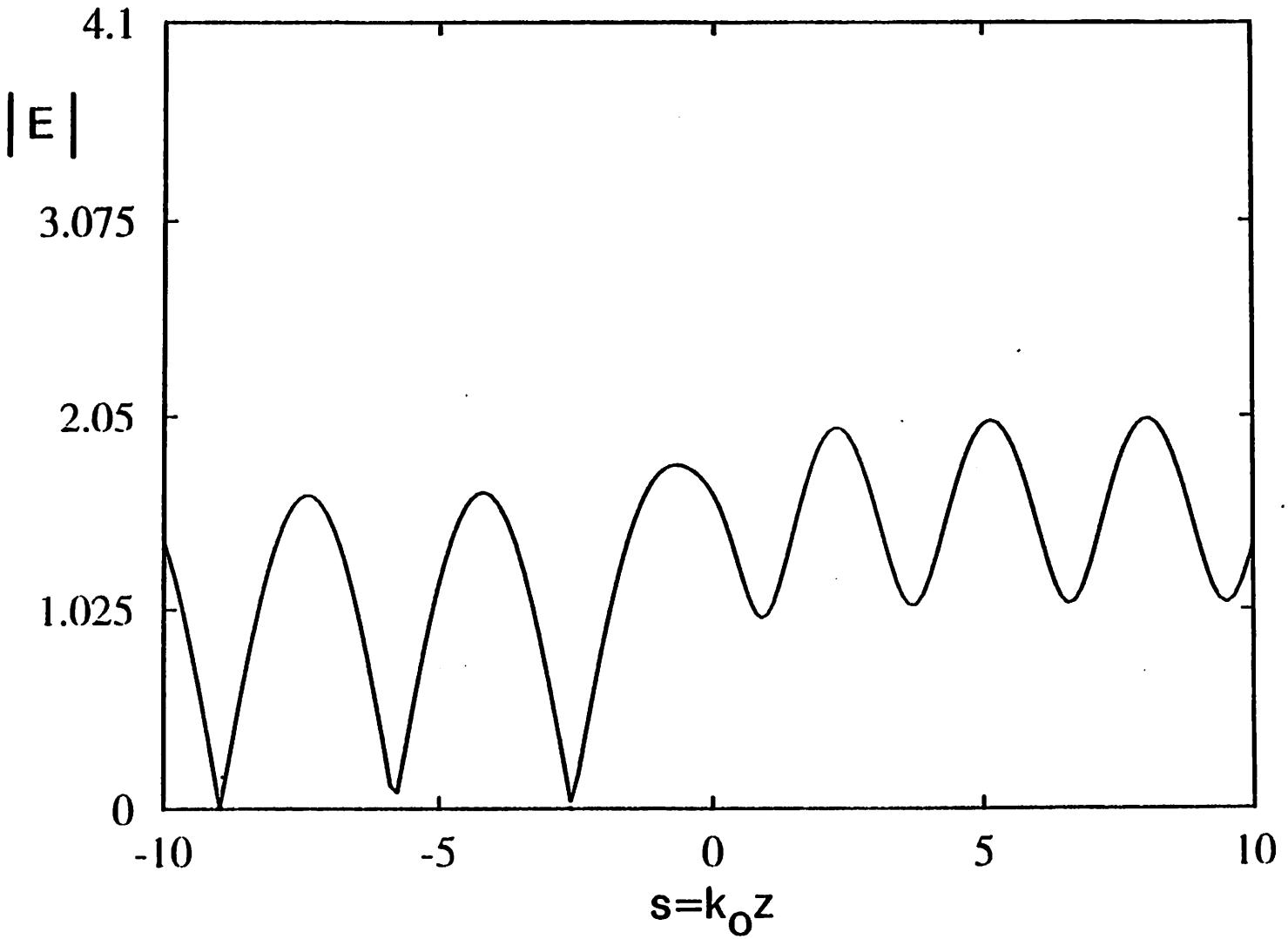

Figure 4a

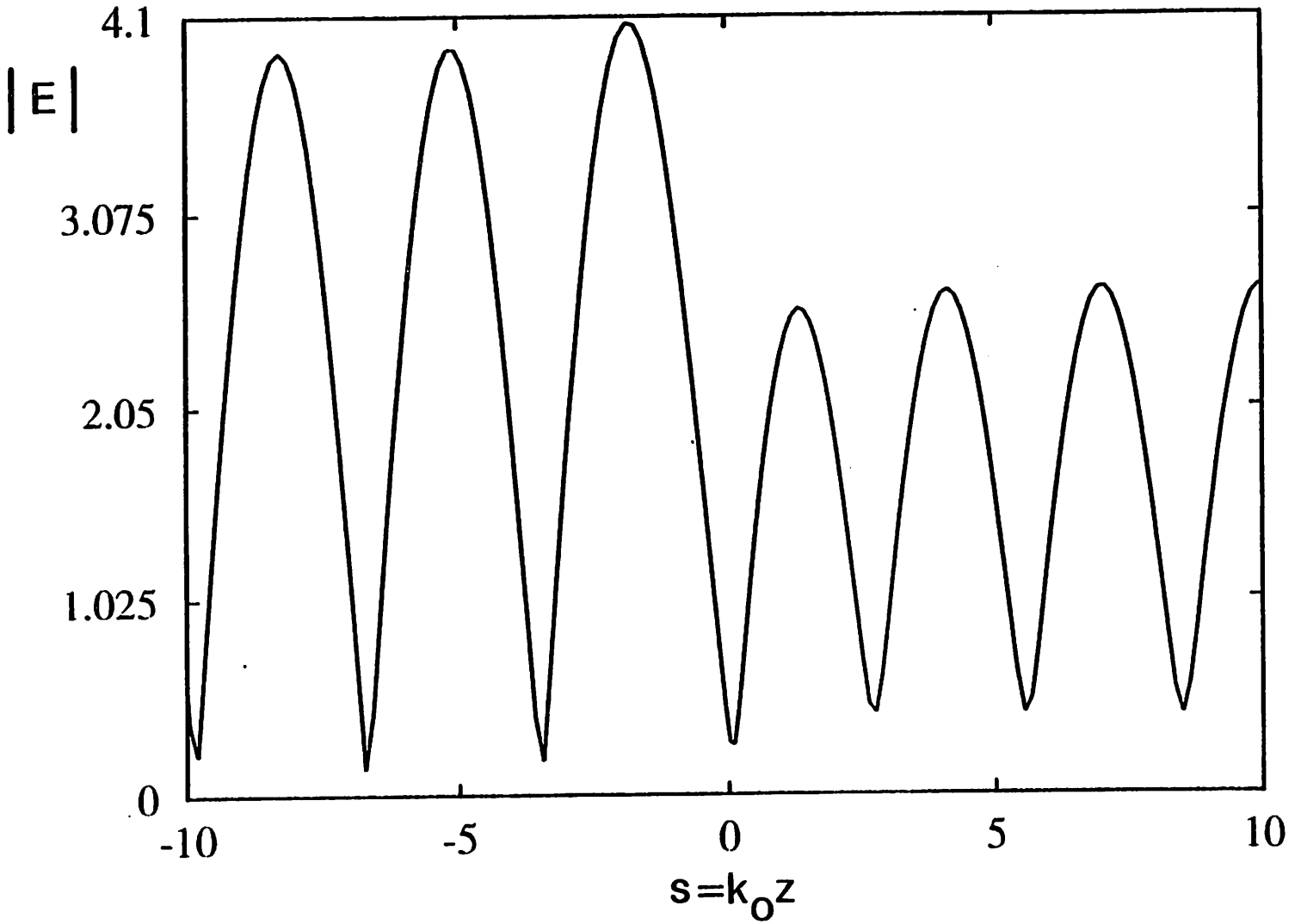

Figure 4b

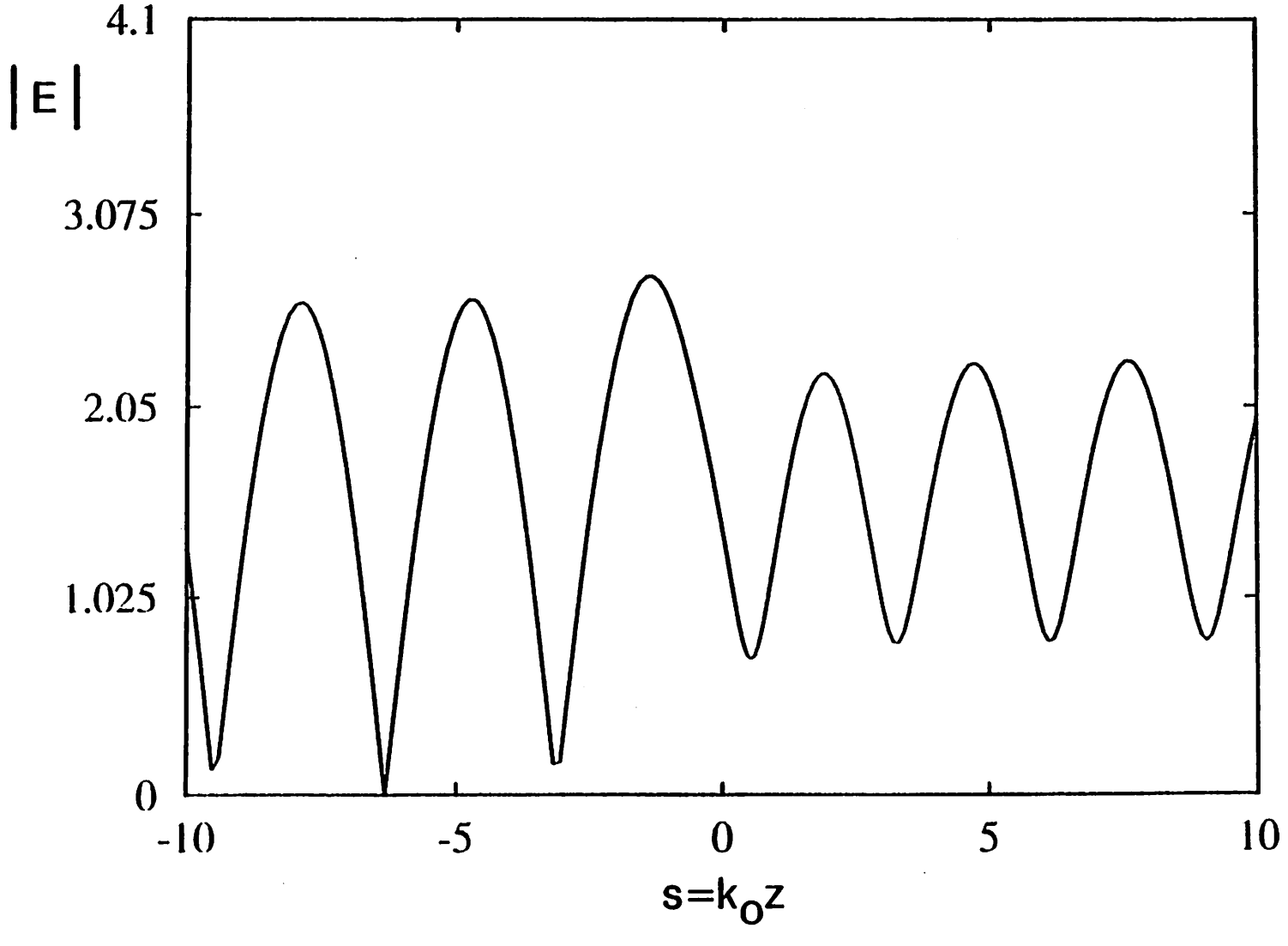

Figure 4c

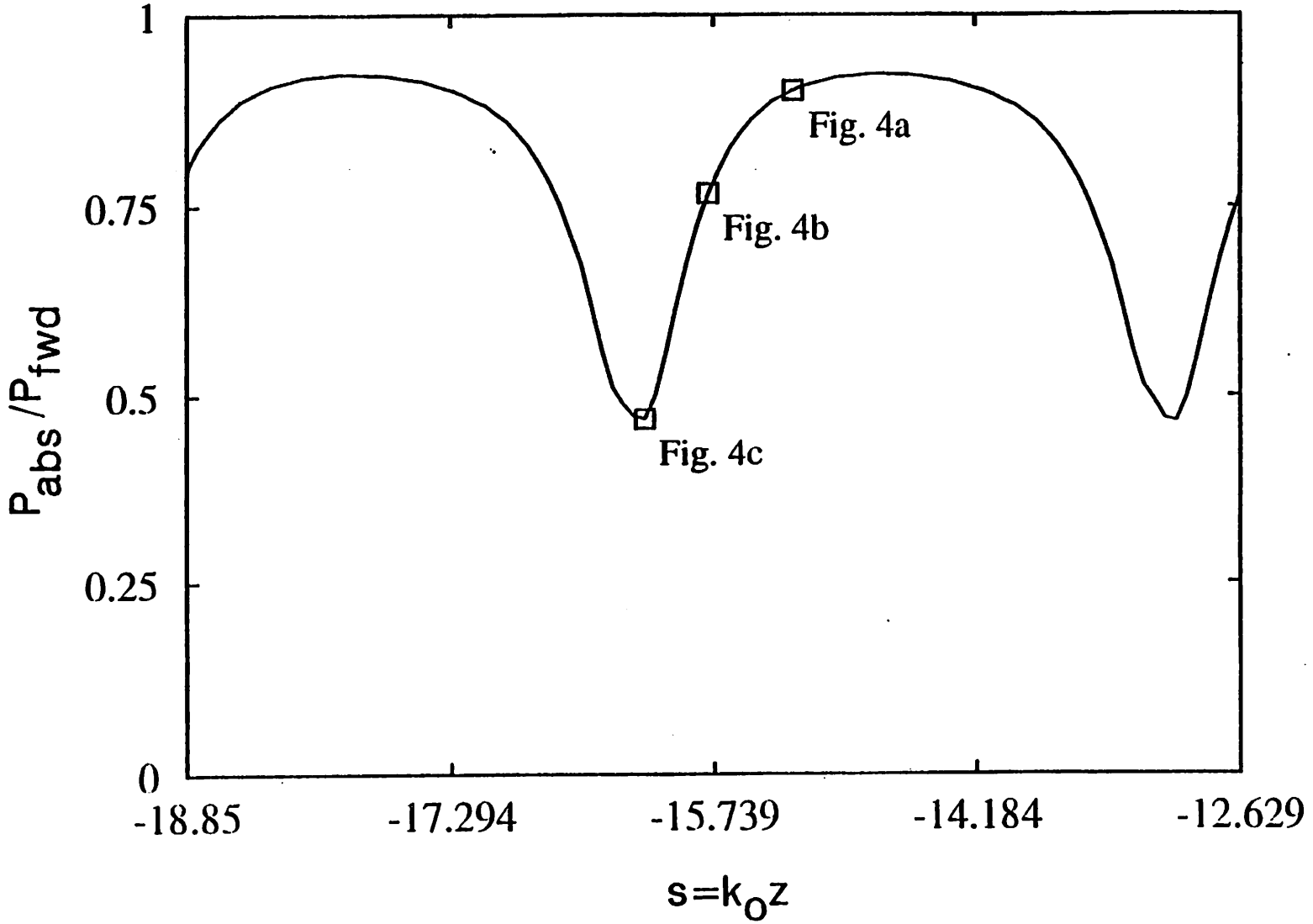
1
0.75
0.5
0.25
0
P_{abs}/P_{fwd}
Fig. 4a
Fig. 4b
Fig. 4c
-18.85
-17.294
-15.739
-14.184
-12.629
$s=k_0z$

Figure 5

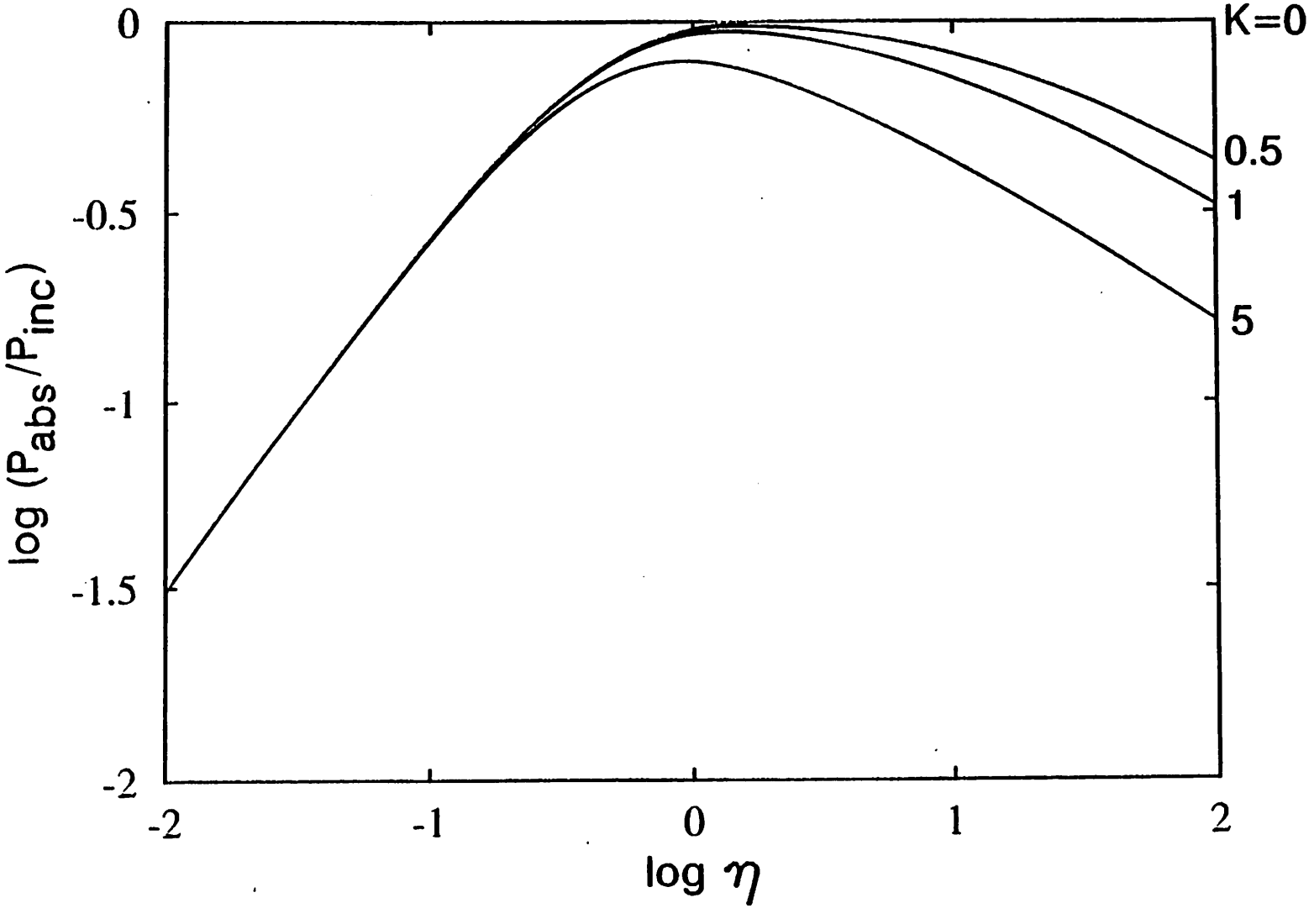

Figure 6

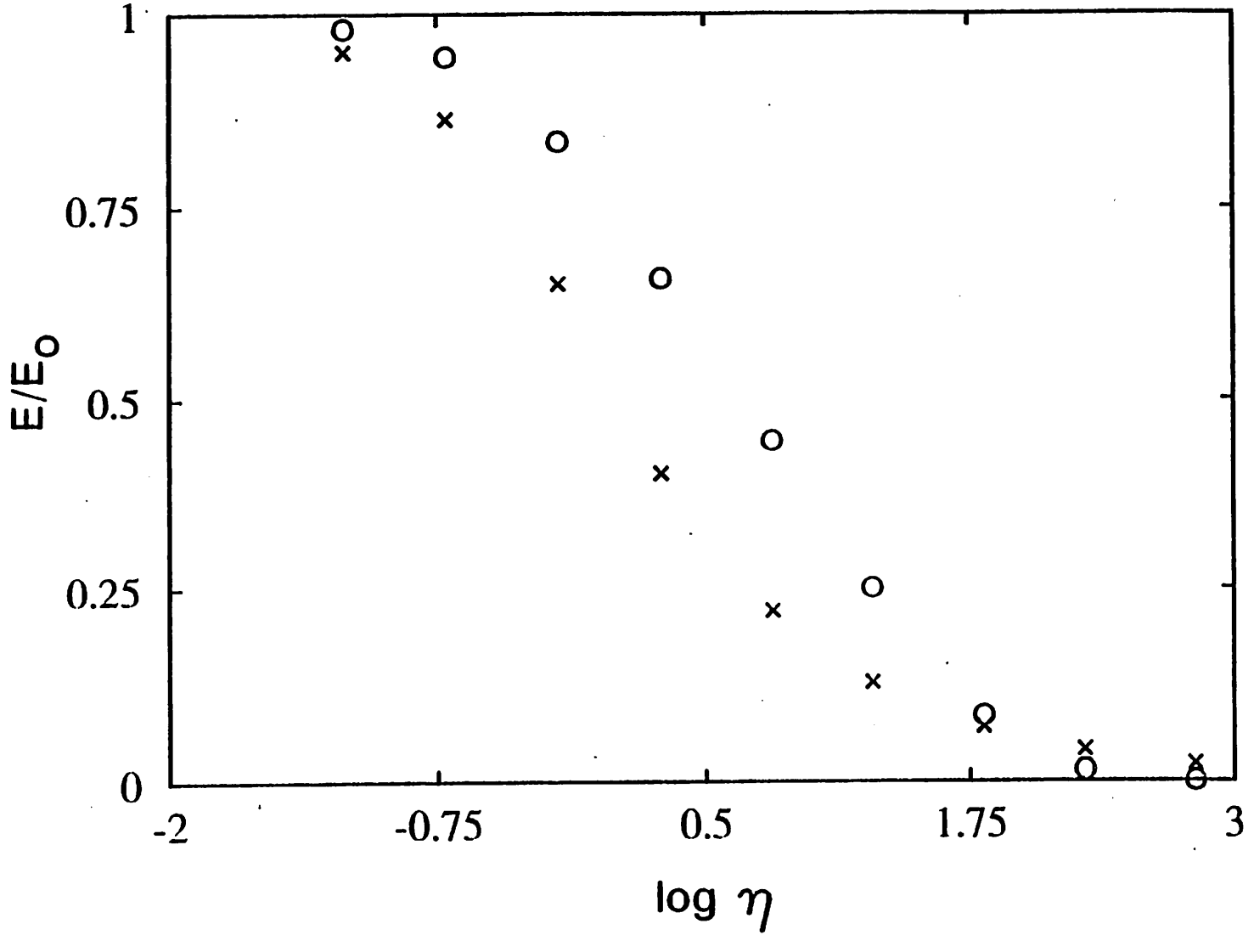

Figure 7

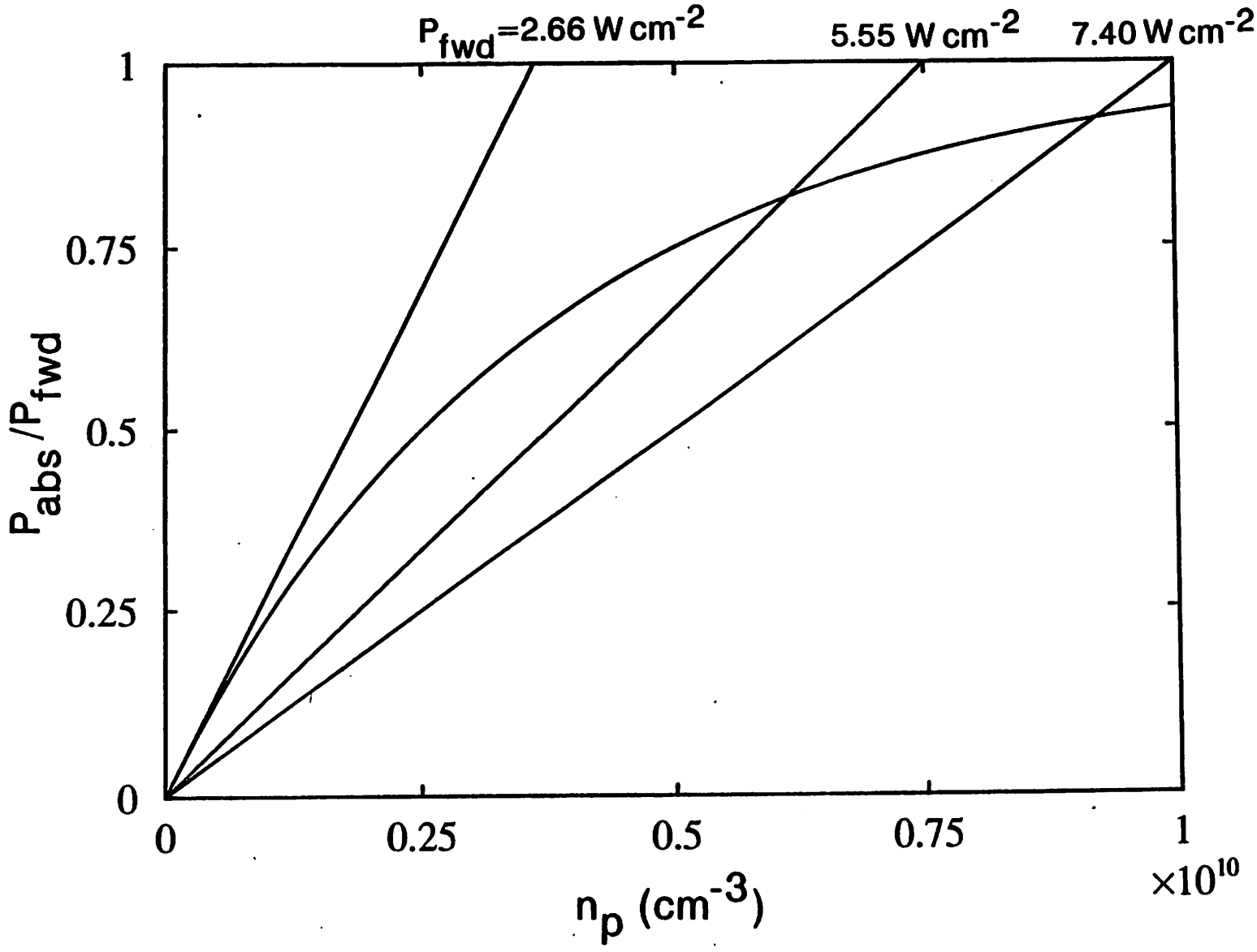
P_{fwd}=2.66 W cm^{-2}
5.55 W cm^{-2}
7.40 W cm^{-2}
1
0.75
0.5
0.25
0
P_{abs}/P_{fwd}
0
0.25
0.5
0.75
1
×10^{10}
n_p (cm^{-3})

Figure 8

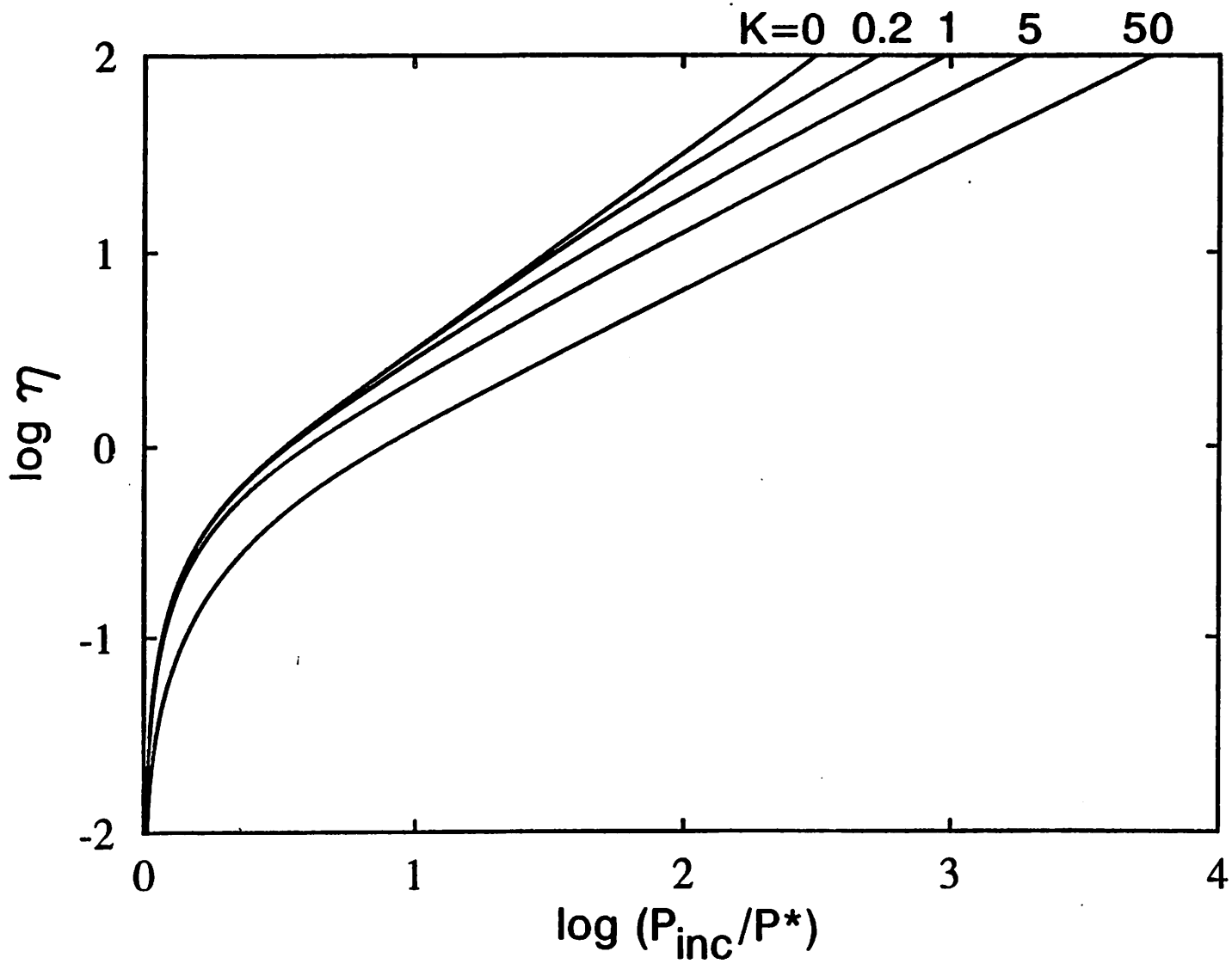

Figure 9